# Detection of tree rot in living trees

ECMI Modelling week, August 2006

Gillian Carson [a], Ivana Manic [b], Maxim Pisarenco [c],  Li Li [d], Philip Reutersward [e] and Maria Sandsten (Instructor) [e]

[a] *University of Strathclyde, Glasgow, UK;*  [b] *University of Novi Sad, Serbia;* [c] *TU Kaiserslautern, Germany;*  [d] *TU Eindhoven, The Netherlands;*  [e] *Lund University, Sweden;*

### Abstract

Root rot, or *Heterogenous annosum*, is a common fungal disease affecting Norway spruce trees, *picea abies*. One of the many non-destructive methods to test for this disease is by using a hammer to impact the outer surface of the tree trunk, and use an accelerometer to receive the consequent vibrations to be analysed. A theoretical model of a decayed tree, with a hole in the centre, and a healthy tree, are constructed. Modelled as spherical cylinders in the radial-tangential plane, elastic wave equations are discretized and boundary conditions applied in each case. Both models are then compared and the results analysed.

## Introduction

A large percentage of harvested Norway spruce (*picea abies*) trees are victims of decay which renders them useless from an economical point of view. Annual losses are estimated at 4.4 million $m^3$ of timber in the northwestern United States and in British Columbia. In 2001, spruce losses in Sweden caused by decay was equivalent to 15% of the annual harvest, which amounts to an annual loss of US $ 100 million, [1].

Wood decay can be caused by fungi such as *Heterobasidion annosum*. *H. annosum* has the most economic impact as it penetrates the central core of the tree trunk even though the infection of the fungi spores occur mostly at root level. The roots can be damaged, for example, by heavy vehicles or animals, which consequently leads to the protective shield of the bark being penetrated [1]. Infection can spread in various ways: via the root system from neighbouring trees, and also via some destructive methods for testing for tree rot such as drilling holes in the tree trunk leaving the core of the tree succeptable to infection. Since *H. annosum* can survive up to 60 years saprophytically, meaning it grows and derives it's nourishment from dead or decaying organic matter, it becomes imperative that research into this fungi, and methods to detect it, are a priority.

1

*H. annosum* flows from the roots upwards and with water being found at the front of growth where the fungi is active, the cell structure begins to break down and hence the wood begins to decay. One of the main problems is that since the sapwood in a living tree is more resistant to decay than the internal heartwood, the tree rot is caused by fungi entering it's host via the root system, leaving no external indications of the decay.

There are two types of methods to detect root rot: destructive testing and non-destructive testing (NDT). Destructive methods include drilling a sample from the tree trunk to examine it's core, although this exposes the tree to further infection, [2]. The most drastic destructive method, however, is to simply fell the tree. There are also various methods existing to use NDT to detect root rot in living trees. Some examples of these include applying ground penetrating radar (GPR) which produces a picture of the inside of the trunk, hence the ability to detect decay, [3]. Vibration methods such as using ultrasound are common, [2], where the signals are transmitted into the trunk from one or more sources such as piezo-electric transducers and then received and analysed, [5], [6]. Other examples of this type of method are given by [4] discussing vibrational techniques with regards to frequency and time domain measurements, and [8] utilizing ultrasonic tomography. The Relative Impedance in Situ Examination (RISE) method is also employed in some cases, where a current is applied to the tree trunk and received and it is noted that the voltage difference of a decayed tree is less of that of a healthy tree, [1]. The resistivity of the tree is determined from this voltage difference. In our case, a hammer is used to induce an excitation force which generates impulse responses. These responses are then received by strategically placed accelerometers and analysed. This method avoids the risk of further infection, is cheaper than some other methods, and is a portable method which makes it extremely useful for taking real life measurements, [7].

In this report, Section one outlines the method adapted from [6]. Section two continues by describing the discretization adapted from [7]. Boundary conditions are then produced in Section three, with implementation and results in Section four. Finally, conclusions are made and future work discussed.



hammer impact

growth-rings

decay in core

PSfrag replacements

accelerometer
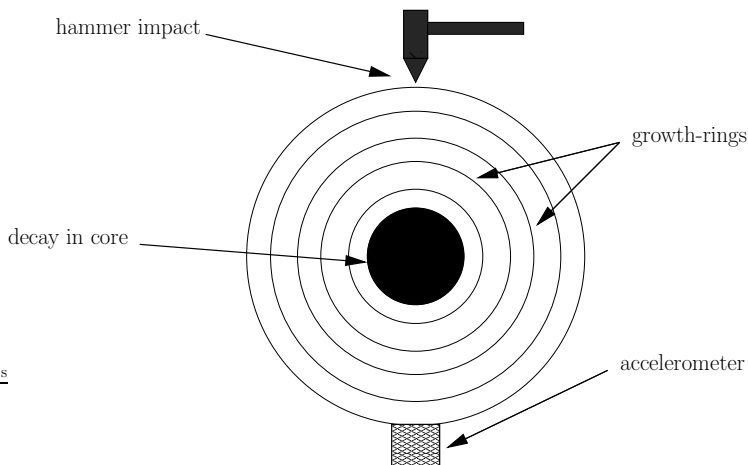
Figure 1: The model depiction.

# 1 The Method

Our aim is to produce a mathematical model to detect tree rot in living trees using an NDT method. By considering a tree trunk to be a circular cylinder, we apply a force using impact-hammer excitation on one point of the curved boundary. We then place one or more accelerometers at positions around the trunk and use these to detect the tree vibrations. By measuring the arrival time of these waves we can consequently estimate whether the tree is healthy or decayed. See Figure 1.

If we consider the propagation of elastic waves in an anisotropic material with curved boundaries, no analytical solution exists and so we have to use a numerical method [6]. In this case, we choose the finite-difference-time domain (FDTD) method since this is the most common for modelling elastic wave propagation. This method is derived from Maxwell's equations and is a special case of the finite difference method. It is essentially a time-stepping method and can be used in one-, two- or three-dimensions, [9]. In our case, we consider the radial-tangential plane, and therefore modelling in two-dimensions is sufficient.

We consider the "ideal" tree trunk to have a perfectly circular cross-section, with growth-rings also circular and uniformly spaced. The co-ordinate system implemented is depicted in Figure 2.
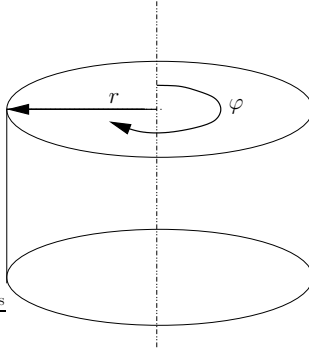


Figure 2: The co-ordinate system.

If we assume that the material is homogeneous, [6] give the elastic wave equations in cylindrical co-ordinates as

$$\rho \frac{\partial^2 u_r}{\partial t^2} = \frac{\partial \tau_{rr}}{\partial r} + \frac{1}{r}\frac{\partial \tau_{r\varphi}}{\partial \varphi} + \frac{\tau_{rr} - \tau_{\varphi\varphi}}{r}, \tag{1}$$

$$\rho \frac{\partial^2 u_\varphi}{\partial t^2} = \frac{\partial \tau_{r\varphi}}{\partial r} + \frac{1}{r}\frac{\partial \tau_{\varphi\varphi}}{\partial \varphi} + \frac{2\tau_{r\varphi}}{r}, \tag{2}$$

where $u_r$ and $u_\varphi$ are displacement components in the radial and spatial directions respectively. $\tau_{rr}$ and $\tau_{\varphi\varphi}$ are the normal stresses, $\tau_{r\varphi}$ is the shear stress and $\rho$ is the density of the material. [6] also outlines the relationship between the stresses $\underline{\tau}$ and strains $\underline{\epsilon}$ of linear elastic anisotropic material as

$$\underline{\tau} = \underline{\mathbf{C}}.\underline{\epsilon}, \tag{3}$$

3

but due to the fact that we are considering the two-dimensional radial-tangential plane, stresses and strains in the $z$-direction can be neglected. Since wood is an orthotropic material, meaning that it has different properties in all three orthogonal directions, we can write the stress-strain relations for the "ideal" tree trunk to be

$$
\begin{bmatrix} \tau_{rr} \\ \tau_{\varphi\varphi} \end{bmatrix} = \begin{bmatrix} C_{22} & C_{23} \\ C_{32} & C_{33} \end{bmatrix} \begin{bmatrix} \epsilon_{rr} \\ \epsilon_{\varphi\varphi} \end{bmatrix} \tag{4}
$$

$$
\tau_{r\varphi} = 2C_{44}\epsilon_{r\varphi}. \tag{5}
$$

Also, in cylindrical co-ordinates, [6] states the strain relations to be

$$
\epsilon_{rr} = \frac{\partial u_r}{\partial r}, \tag{6}
$$

$$
\epsilon_{\varphi\varphi} = \frac{u_r}{r} + \frac{1}{r}\frac{\partial u_\varphi}{\partial \varphi}, \tag{7}
$$

$$
\epsilon_{r\varphi} = \frac{1}{2}\left(\frac{1}{r}\frac{\partial u_r}{\partial \varphi} + \frac{u_\varphi}{\partial r} - \frac{u_\varphi}{r}\right). \tag{8}
$$

We can then proceed by substituting equations (6)-(8) into equations (4) and (5), and consequently substituting the resulting expressions into the cylindrical two-dimensional elastic wave equations given by equations (1) and (2), we have

$$
\begin{aligned}
\rho\frac{\partial^2 u_r}{\partial t^2} = {} & C_{22}\frac{\partial^2 u_r}{\partial r^2} + \frac{C_{44}}{r^2}\frac{\partial^2 u_r}{\partial \varphi^2} + \frac{1}{r}(C_{23}+C_{44})\frac{\partial^2 u_\varphi}{\partial \varphi \partial r} \\
& - \frac{1}{r^2}(C_{33}+C_{44})\frac{\partial u_\varphi}{\partial \varphi} + \frac{1}{r}(C_{22}+C_{23}-C_{32})\frac{\partial u_r}{\partial r} - \frac{C_{33}}{r^2}u_r,
\end{aligned} \tag{9}
$$

$$
\begin{aligned}
\rho\frac{\partial^2 u_\varphi}{\partial t^2} = {} & \frac{C_{33}}{r^2}\frac{\partial^2 u_\varphi}{\partial \varphi^2} + C_{44}\frac{\partial^2 u_\varphi}{\partial r^2} + \frac{1}{r}(C_{32}+C_{44})\frac{\partial^2 u_r}{\partial \varphi \partial r} \\
& + \frac{1}{r^2}(C_{33}+C_{44})\frac{\partial u_r}{\partial \varphi} + \frac{C_{44}}{r}\frac{\partial u_\varphi}{\partial r} - \frac{C_{44}}{r^2}u_\varphi.
\end{aligned} \tag{10}
$$

In the next section, we describe the discretization of equations (9) and (10).

## 2 Discretization

The partial differential equations (9) and (10) are written only in terms of the stiffness components $\underline{\mathbf{C}}$ and the displacement components $u_r$ and $u_\varphi$ and are discretized using central differences in time and space. Applying a staggered grid as shown in Figure 3 to develop discretization rules (see Appendix), we can rewrite equation (9) as

$$
\begin{aligned}
\rho\frac{1}{\Delta t^2}(u_{r_{i,k}}^{n+1} - 2u_{r_{i,k}}^{n} + u_{r_{i,k}}^{n-1}) = {} & (a+b)u_{\varphi_{i-1,k}}^{n} - (a+b)u_{\varphi_{i,k}}^{n} + (b-a)u_{\varphi_{i-1,k+1}}^{n} \\
& + (a-b)u_{\varphi_{i,k+1}}^{n} + (c-d)u_{r_{i,k-1}}^{n} + (c+d)u_{r_{i,k+1}}^{n} \\
& + e\,u_{r_{i-1,k}}^{n} + e\,u_{r_{i+1,k}}^{n} - (2c+2e+f)u_{r_{i,k}}^{n},
\end{aligned} \tag{11}
$$

4
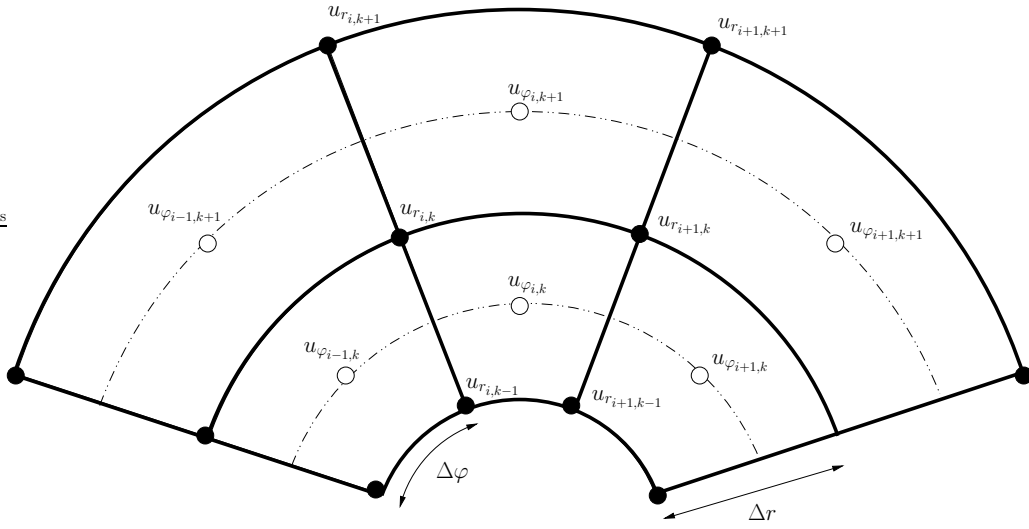
Figure 3: The staggered grid.

where

$$a = \frac{C_{23} + C_{44}}{k(\Delta r)^2 \Delta \varphi}, \qquad d = \frac{C_{23} + C_{22} - C_{32}}{2k(\Delta r)^2},$$

$$b = \frac{C_{33} + C_{44}}{2(k\Delta r)^2 \Delta \varphi}, \qquad e = \frac{C_{44}}{(k\Delta r)^2 \Delta \varphi^2},$$

$$c = \frac{C_{22}}{\Delta r^2}, \qquad f = \frac{C_{33}}{(k\Delta r)^2}.$$

Equation (10) can be rewritten as

$$
\begin{aligned}
\rho \frac{1}{\Delta t^2}(u_{\varphi_{i,k}}^{n+1} - 2u_{\varphi_{i,k}}^{n} + u_{\varphi_{i,k}}^{n-1}) = & -g u_{\varphi_{i-1,k}}^{n} + (g - 2h - 2m - \frac{n}{k})u_{\varphi_{i,k}}^{n} - \frac{n}{2}u_{\varphi_{i-1,k+1}}^{n} \\
& + (h + m + \frac{n}{2})u_{\varphi_{i,k+1}}^{n} + (h + m)u_{\varphi_{i,k-1}}^{n} - 2m u_{\varphi_{i+1,k}}^{n} \\
& + m u_{\varphi_{i+1,k-1}}^{n} + m\, u_{\varphi_{i+1,k+1}}^{n} + (q - v)\, u_{r_{i-1,k}}^{n} \\
& - 2q u_{r_{i,k}}^{n} + q\, u_{r_{i-1,k+1}}^{n} + q u_{r_{i,k+1}}^{n} + v u_{r_{i+1,k}}^{n}, \qquad (12)
\end{aligned}
$$

where

$$g = \frac{C_{44}}{2k(\Delta r)^2}, \qquad n = \frac{C_{44}}{k(\Delta r)^2},$$

$$h = \frac{C_{44}}{\Delta r^2}, \qquad q = \frac{C_{32} + C_{44}}{k(\Delta r)^2 \Delta \varphi},$$

$$m = \frac{C_{33}}{2(k\Delta r)^2 \Delta \varphi^2}, \qquad v = \frac{C_{33} + C_{44}}{2(k\Delta r)^2 \Delta \varphi},$$

Now that we have the wave equations in discretized form, we can continue in the next section to consider the boundary conditions.
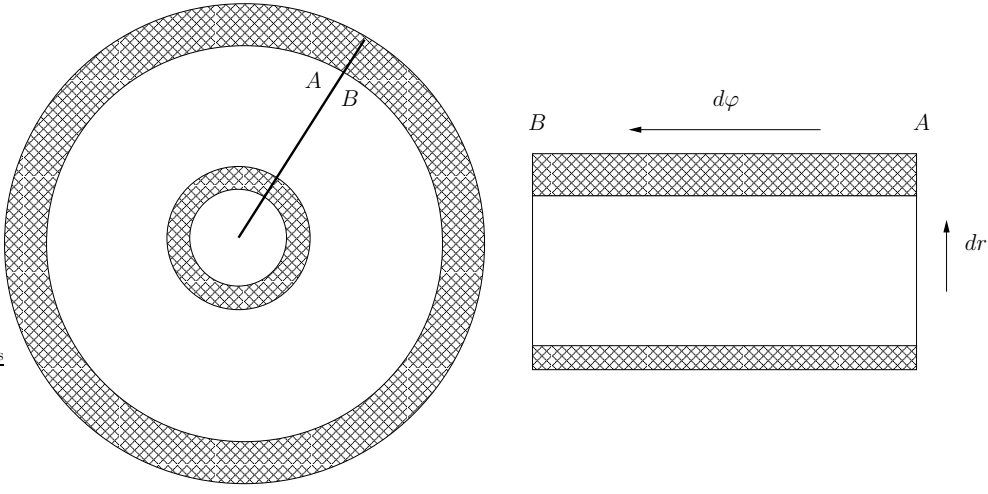
Figure 4: Boundary condition notation.

# 3   Boundary Conditions

We now need to calculate the boundary conditions on the outer and inner boundaries. Since, from the discretization rules (see Appendix), we require the derivatives of the points $u_{r_{l,m}}$ and $u_{\varphi_{l,m}}$ with $l = 0, 1...i$, $m = 0, 1...k$, we must therefore introduce a fictitious layer on each of the boundaries. See Figure 4.

We assume that the inner boundary layer is stress-free for both a healthy tree and a decayed tree, [6], [7], hence we can apply

$$\tau_{rr} = 0. \tag{13}$$

Then, from equations (4), (6) and (7) and with (13) we obtain,

$$C_{22} \frac{\partial u_r}{\partial r} = -\frac{C_{23}}{r} \left( u_r + \frac{\partial u_\varphi}{\partial \varphi} \right). \tag{14}$$

We continue by discretizing (see Appendix) and rearranging the resulting equation for the element $u_{r_{i,k-1}}^n$ (see Figure 5 (a)), which represents the fictitious inner boundary condition we require as

$$u_{r_{i,k-1}}^n = u_{r_{i,k+1}}^n + \frac{2C_{23}}{kC_{22}} \left[ u_{r_{i,k}}^n + \frac{1}{2\Delta\varphi} \left( u_{\varphi_{i,k+1}}^n + u_{\varphi_{i,k}}^n - u_{\varphi_{i-1,k+1}}^n - u_{\varphi_{i-1,k}}^n \right) \right]. \tag{15}$$

This gives us $u_r$ on the fictitious layer.

The fictitious outer boundary condition required is calculated in a similar way with one subtle difference: we assume that the outer radius is stress-free at every point except where the hammer excitation impact is exerted, [6]. Hence we must adapt equation (13) so that

$$\tau_{rr} = \begin{cases} 0 & \text{free surface} \\ s(t) & \text{hammer excitation,} \end{cases} \tag{16}$$

6
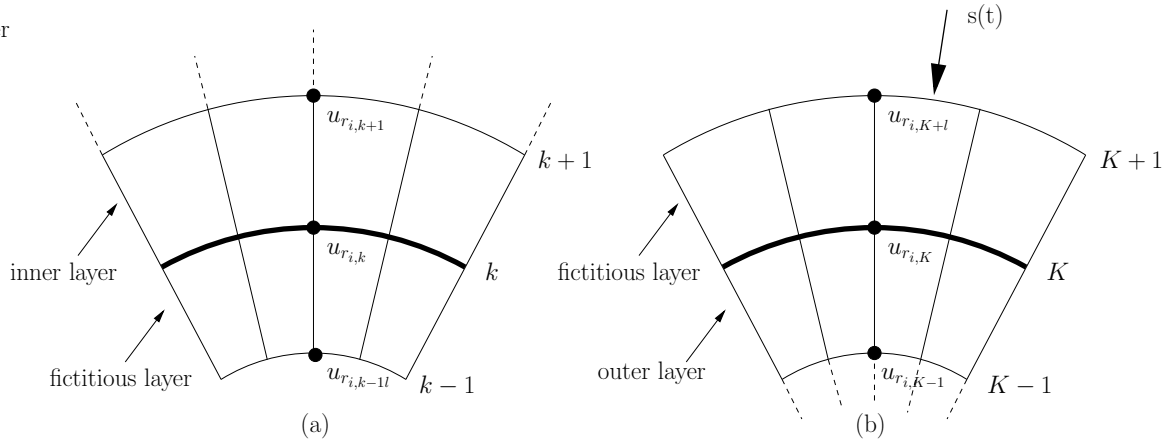
Figure 5: (a)-inner boundary layer, (b)-outer boundary layer.

Furthermore, we utilize equation (16) along with equations (4), (5) and (6), discretize (see Appendix), and rearrange the resulting equation for the required term $u_{r_{i,K+1}}^{n}$ (see Figure 5 (b)), so that

$$
\begin{aligned}
u_{r_{i,K+1}}^{n} &= \frac{2\Delta r}{C_{22}}\tau_{rr} + u_{r_{i,K-1}}^{n} - \frac{2C_{23}}{KC_{22}}u_{r_{i,K}}^{n} \\
&\quad - \frac{C_{23}}{C_{22}K\Delta\varphi}\left(u_{\varphi_{i,K+1}}^{n} + u_{\varphi_{i,K}}^{n} - u_{\varphi_{i-1,K+1}}^{n} - u_{\varphi_{i-1,K}}^{n}\right).
\end{aligned}
\tag{17}
$$

To get $u_{\varphi}$ on the fictitious layer we assume that we have no displacement in the spatial direction at the boundary, hence we set

$$
u_{\varphi_{i,k-1}} = -u_{\varphi_{i,k}}
$$
$$
u_{\varphi_{i,K+1}} = -u_{\varphi_{i,K}}
$$

on the inner and outer layers respectively. Equation (15) is unchanged and equation (17) can be simplified to

$$
u_{r_{i,K+1}}^{n} = \frac{2\Delta r}{C_{22}}\tau_{rr} + u_{r_{i,K-1}}^{n} - \frac{2C_{23}}{KC_{22}}u_{r_{i,K}}^{n}.
\tag{18}
$$

(a)                                           (b)
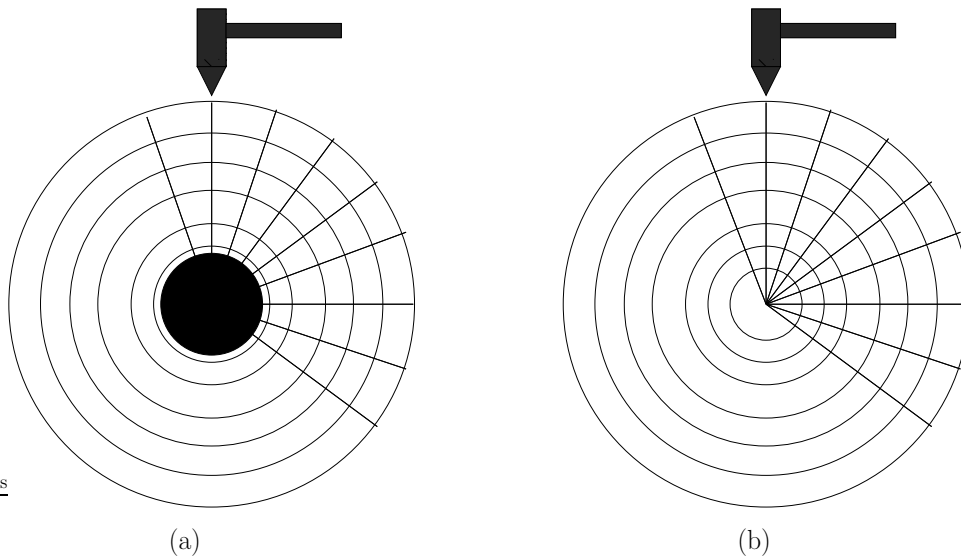
Figure 6: (a) - decayed model, (b) - healthy model.

# 4    Results

Two models were constructed and implemented in the computational package MATLAB. The first describes a decayed tree, (see Figure 6 (a)), which consists of a hole in the core to represent the tree rot. The second model describes a healthy tree, (see Figure 6 (a)), which has no hole although the centre point must be treated cautiously. Each of the models also utilize the same impact forcing function shown in Figure 7 in the time domain.
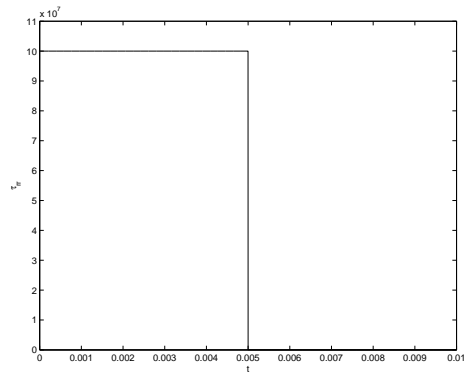


Figure 7: Impact force of the hammer in the time domain.

## 4.1    The decayed tree model

The decayed tree model includes a hole in the central core representing the tree rot and is implemented using the discretized elastic wave equations (11) and (12), the boundary conditions (15), and (18) previously described and the discretization grid pictured in

8
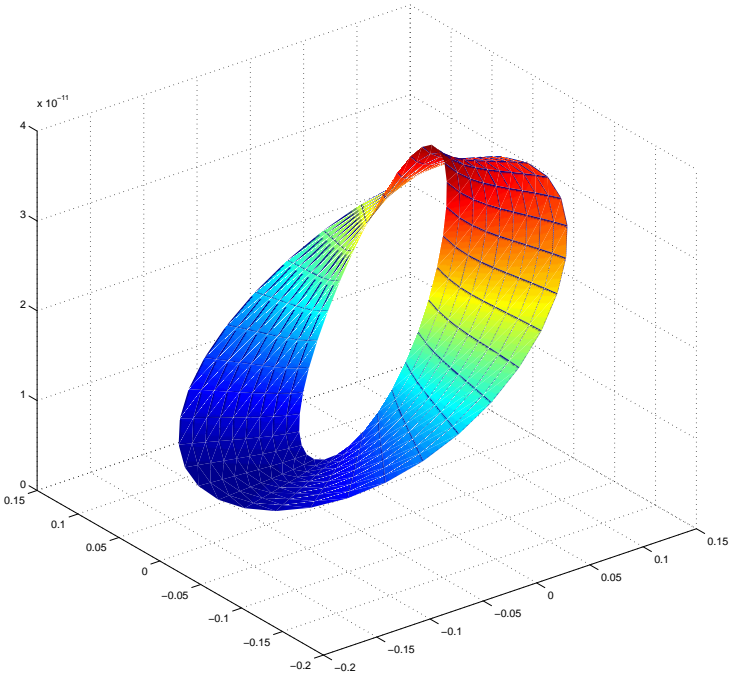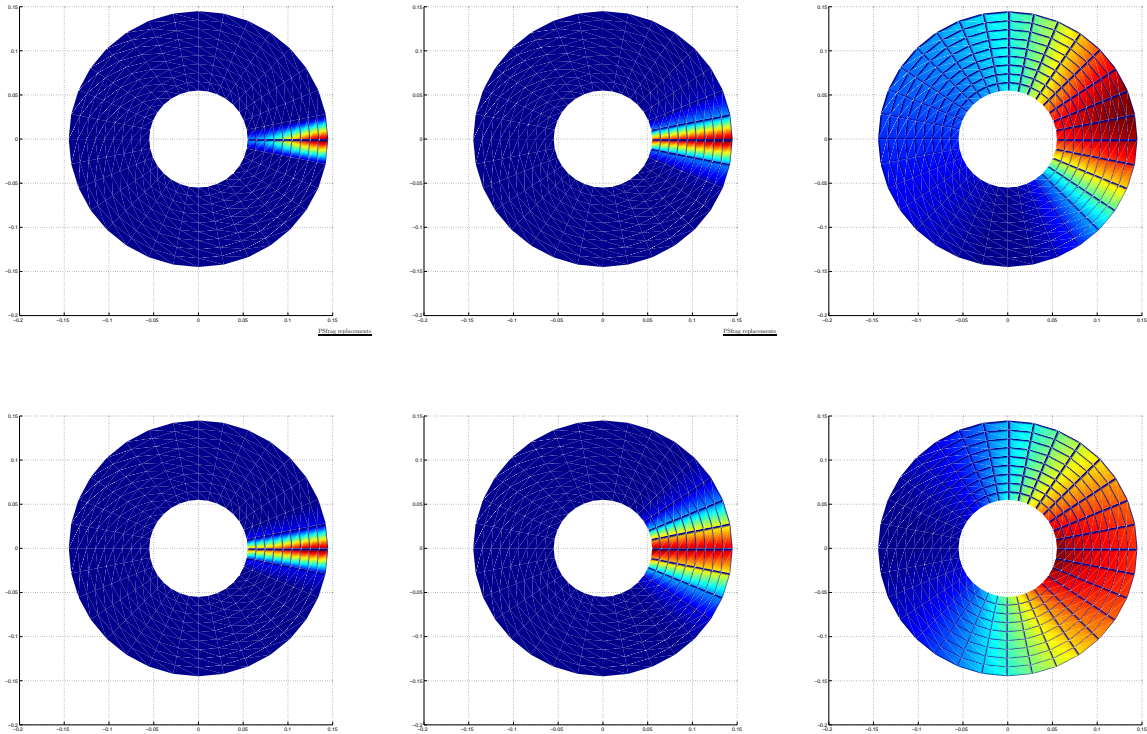
Figure 3.

Figure 8: 3D still of decayed model.

9

The top row of figures show the decayed tree model for the isotropic case with the unit stress tensor constants whilst the second row of figures give the case described by equation (4), [6]. The figures were produced by interupting the model at three separate time steps, $t = 2s$, $t = 20s$ and $t = 400s$.

## 4.2    The healthy tree model
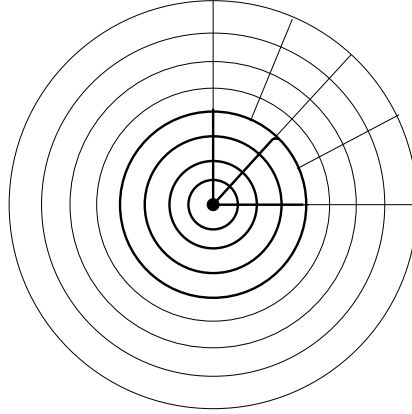


Figure 9: Healthy tree discretization grid.
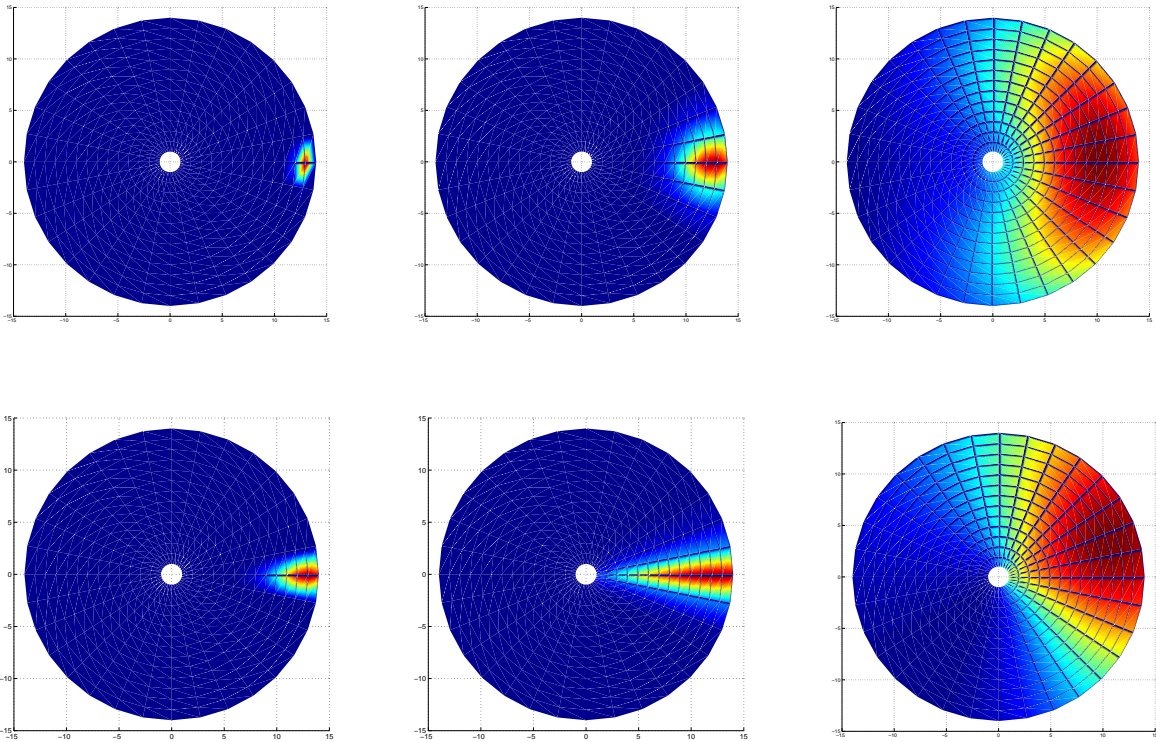


Since the central core of a healthy tree should not have a hole, the case of a healthy tree poses the different problem of a singularity at this centre point position, [6]. However,to bypass this issue, the easiest solution is to include a hole but on a very small scale. In

10

terms of the cells for our grid, as the radius decreases, less cells are necessary. Very small cells would also mean that we would have to use smaller time steps, due to numerical considerations. Hence the cells tending towards the centre point become so small that two cells are merged. Interpolation is then applied to calculate the $\underline{u}$ components, needed by the numerical scheme, in the regions where cells have been merged. The new discretization grid is constructed as demonstrated in Figure 9.

Similar to the decayed model, the top row of figures show the healthy tree model for the isotropic case with the unit stress tensor constants, whilst the second row of figures give the case described by equation (4), [6]. Again the figures were produced by interupting the model at three separate time steps, $t = 2s$, $t = 20s$ and $t = 400s$ in order to compare them with the decayed model figures. In the next section we will compare these similarities and differences and discuss the results.
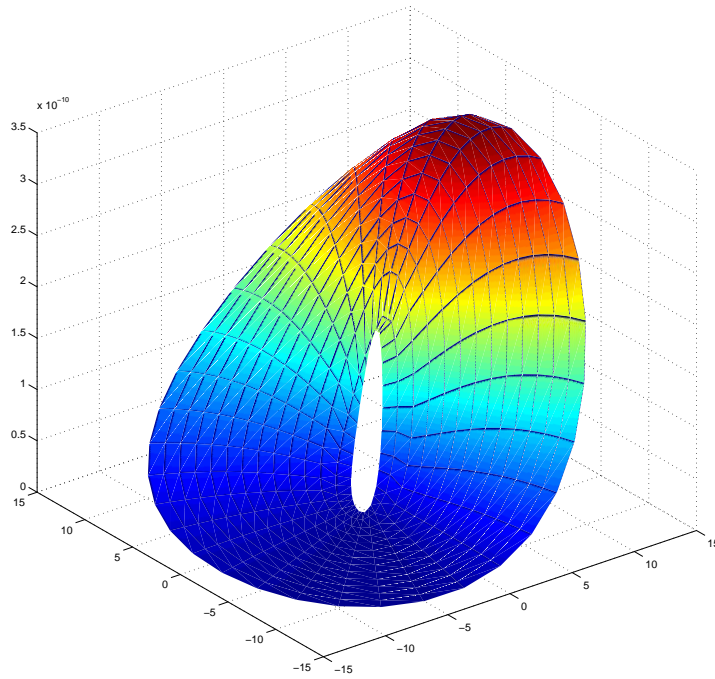


Figure 10: 3D still of healthy model.

## 4.3 Comparison of the models

The models are compared in two ways. Firstly, we compare the healthy model with the decayed model in general, and secondly compare the change in stress-tensor constants.

The main general result is that, for the decayed model, the wave is reflected back from the inner boundary of the cavity resulting in an increased wave velocity in the angular, or $\varphi$, direction. The wave will therefore be received by the accelerometer faster in a decayed

tree, implying that the hammer excitation method is a valid method according to our model.

By varying the stress tensor constants for each of the models, we can deduce that the isotropic case for the healthy tree produces a circular wave. This is not the case with the decayed isotropic model and a full explanation requires further time and investigation. In the other three instances, we can see that the wave takes a triangular form and this is also noted in [6].

Another major observation is that there is a drift in the angular direction when the constants are varied. Although this is not immediately obvious in the healthy isotropic case, we may suggest that it does occur but to a smaller degree. This drift also seems to change direction depending on the stress tensor constants and we must conclude that, again, further investigation is required for a full explanation.

# Conclusion

The aim of this project was to use the NDT hammer excitation method to construct a model to detect decay in living trees. Two models have been created and implemented: one modelling a decayed tree and another modelling a healthy tree. These were then compared and discussed. Results indicate that, due to the faster wave propagation in the angular direction of the decayed model, the wave will therefore be received faster by the accelerometer. This suggests that this method is valid, and could be tested further by comparing with real experimental data. Due to time restraints, insufficient simulations were performed and analysed to determine, for example, the influence of different parameters such as the stress tensor, $\underline{\mathbf{C}}$, or to explain the wave drift in the angular direction. Consequently this is suggested as future work.

# Appendix

Discretization rules:

$$
\begin{aligned}
\frac{\partial^2 u_r}{\partial t^2} &= \frac{1}{\Delta t^2}\left(u_{r_{i,k}}^{n+1} - 2u_{r_{i,k}}^{n} + u_{r_{i,k}}^{n-1}\right), \\
\frac{\partial^2 u_\varphi}{\partial t^2} &= \frac{1}{\Delta t^2}\left(u_{\varphi_{i,k}}^{n+1} - 2u_{\varphi_{i,k}}^{n} + u_{\varphi_{i,k}}^{n-1}\right), \\
\frac{\partial^2 u_r}{\partial r^2} &= \frac{1}{\Delta r^2}\left(u_{r_{i,k+1}}^{n} - 2u_{r_{i,k}}^{n} + u_{r_{i,k-1}}^{n}\right), \\
\frac{\partial^2 u_r}{\partial \varphi^2} &= \frac{1}{\Delta \varphi^2}\left(u_{r_{i+1,k}}^{n} - 2u_{r_{i,k}}^{n} + u_{r_{i-1,k}}^{n}\right), \\
\frac{\partial^2 u_\varphi}{\partial r^2} &= \frac{1}{\Delta r^2}\left(u_{\varphi_{i,k+1}}^{n} - 2u_{\varphi_{i,k}}^{n} + u_{\varphi_{i,k-1}}^{n}\right), \\
\frac{\partial^2 u_\varphi}{\partial \varphi^2} &= \frac{1}{2\Delta \varphi^2}\left(u_{\varphi_{i,k+1}}^{n} - 2u_{\varphi_{i,k}}^{n} + u_{\varphi_{i,k-1}}^{n} + u_{\varphi_{i+1,k+1}}^{n} - 2u_{\varphi_{i+1,k}}^{n} + u_{\varphi_{i+1,k-1}}^{n}\right),
\end{aligned}
$$

$$\frac{\partial^2 u_r}{\partial r \partial \varphi} = \frac{1}{\Delta r \Delta \varphi} \left( u^n_{r_{i,k+1}} - 2u^n_{r_{i,k}} + u^n_{r_{i-1,k+1}} + u^n_{r_{i-1,k}} \right),$$

$$\frac{\partial u_r}{\partial r} = \frac{1}{2\Delta r} \left( u^n_{r_{i,k+1}} - u^n_{r_{i,k-1}} \right),$$

$$\frac{\partial u_\varphi}{\partial \varphi} = \frac{1}{2\Delta \varphi} \left( u^n_{\varphi_{i,k+1}} + u^n_{\varphi_{i,k}} - u^n_{\varphi_{i-1,k+1}} - u^n_{\varphi_{i-1,k}} \right),$$

$$\frac{\partial^2 u_\varphi}{\partial r \partial \varphi} = \frac{1}{\Delta r \Delta \varphi} \left( u^n_{\varphi_{i,k+1}} - u^n_{\varphi_{i,k}} - u^n_{\varphi_{i-1,k+1}} + u^n_{\varphi_{i-1,k}} \right),$$

$$\frac{\partial u_r}{\partial \varphi} = \frac{1}{2\Delta \varphi} \left( u^n_{r_{i+1,k}} - u^n_{r_{i-1,k}} \right),$$

$$\frac{\partial u_\varphi}{\partial r} = \frac{1}{2\Delta r} \left( u^n_{\varphi_{i,k+1}} + u^n_{\varphi_{i,k}} - u^n_{\varphi_{i-1,k+1}} - u^n_{\varphi_{i-1,k}} \right).$$

# References

[1] B. LARSSON, B. BENGTSSON AND M. GUSTAFSSON, *Non destructive detection of decay in living trees*, Tree Physiology 24, pp853-858, 2004.

[2] J. BODIG, *The process of NDE research for wood and wood composites*, 12th International Symposium on Non-destructive testing of wood, Vol 6, No. 3, March 2001.

[3] *www.treeradar.com.*

[4] D. OUIS, *Vibrational and acoustical experiments on logs of spruce*, Wood and science technology, **33**, pp151-184, 1999.

[5] X. WANG, R. J. ROSS, J. R. ERICKSON AND J. B. LIGON, *Non-destructive evaluation of trees*, Experimental Techniques, pp27-29, November/December 2000.

[6] S. SCHUBERT, D. GSELL, P. NIEMZ AND J. DUAL, *Numerical simulation of elastic wave propagation in the radial-tangential plane of wooden trunks with and without fungal decay*, 3rd Workshop "NDT in Progress", Prague, 2005.

[7] D. GSELL, T. LEUTENEGGER AND J. DUAL, *Modelling three-dimensional elastic wave propagation in circular cylindrical structures using a finite-difference approach*, J. Acoust. Soc. Am. **116**(6), December 2004.

[8] V. BUCUR, *ultrasonic techniques for non-destructive testing of standing trees*, Ultrasonics **43**, pp237-239, July 2004.

[9] *www.electromagnetics.info/fdtd.*